Deformation of periodic nanovoid structures in Mg single crystals

Materials Research Express

RECEIVED
10 December 2017

REVISED
21 December 2017

ACCEPTED FOR PUBLICATION
10 January 2018

PUBLISHED
24 January 2018

PAPER

Deformation of periodic nanovoid structures in Mg single crystals

Shuozhi Xu[1], **Yanqing Su**[2] and **Saeed Zare Chavoshi**[3]

[1] California NanoSystems Institute, University of California, Santa Barbara, Santa Barbara, CA 93106-6105, United States of America
[2] Department of Mechanical Engineering, University of California, Santa Barbara, Santa Barbara, CA 93106-5070, United States of America
[3] Department of Mechanical Engineering, Imperial College London, London SW7 2AZ, United Kingdom

E-mail: shuozhixu@ucsb.edu

Keywords: molecular dynamics, magnesium, nanovoid, deformation

Abstract

Large scale molecular dynamics (MD) simulations in Mg single crystal containing periodic cylindrical voids subject to uniaxial tension along the z direction are carried out. Models with different initial void sizes and crystallographic orientations are explored using two interatomic potentials. It is found that (i) a larger initial void always leads to a lower yield stress, in agreement with an analytic prediction; (ii) in the model with $x[\bar{1}100]$–$y[0001]$–$z[11\bar{2}0]$ orientations, the two potentials predict different types of tension twins and phase transformation; (iii) in the model with $x[0001]$–$y[11\bar{2}0]$–$z[\bar{1}100]$ orientations, the two potentials identically predict the nucleation of edge dislocations on the prismatic plane, which then glide away from the void, resulting in extrusions at the void surface; in the case of the smallest initial void, these surface extrusions pinch the void into two voids. Besides bringing new physical understanding of the nanovoid structures, our work highlights the variability and uncertainty in MD simulations arising from the interatomic potential, an issue relatively lightly addressed in the literature to date.

1. Introduction

Nano/micro-scale voids play an important role in ductile fracture of metallic materials [1]. Subject to tensile loading, voids nucleate from 'hot spots' in an otherwise void-free metal, e.g., grain boundaries, precipitate/matrix interfaces; then voids grow and coalesce with each other, forming macroscopically observable cracks and eventually resulting in failure of the material [2]. Even with negligible growth and coalescence, the existence of voids alone may contribute to strain hardening because they are barriers to dislocation movement [3]. Therefore, it is necessary to explore deformation of metals containing voids to elucidate their mechanical responses.

Early work of void growth was conducted in the classical continuum mechanics framework, some of which focused on formulating damage functions [4, 5]. However, it is known that the continuum assumption no longer holds for problems at the nano/micron length scale, e.g., nanovoids, which may exhibit a strong size effect that is not included in local continuum-based constitutive relations. As high-performance computing resources are increasingly accessible to researchers, direct atomistic modeling methods such as molecular dynamics (MD) have become a popular choice in exploring nanovoids in metallic materials, leading to several nanovoid growth mechanisms [6, 7] that are otherwise difficult to identify in *in situ* experiments [8].

Prior atomistic studies revealed that the nanovoid growth process is affected by many factors, including, but not limited to, strain rate [9], temperature [10], initial porosity [11], initial void shape [12], and crystallographic orientations [13–15]. Compared with face-centered cubic (FCC) [1, 10, 12] and body-centered cubic (BCC) [2, 9, 11] systems, there exist much fewer studies of nanvoids in metals with a hexagonal close-packed (HCP) lattice, in part due to a lack of reliable interatomic potential and more complicated slip/twinning systems in the latter. Particularly for HCP Mg, the lightest and the third most abundant element in the Earth's crust among all metals, most atomistic simulations in the literature concerned nanocracks [16–19]; to the best of our knowledge, only a few MD and atomistic-based multiscale studies have been devoted to nanovoids [20–22]. Since cracks and

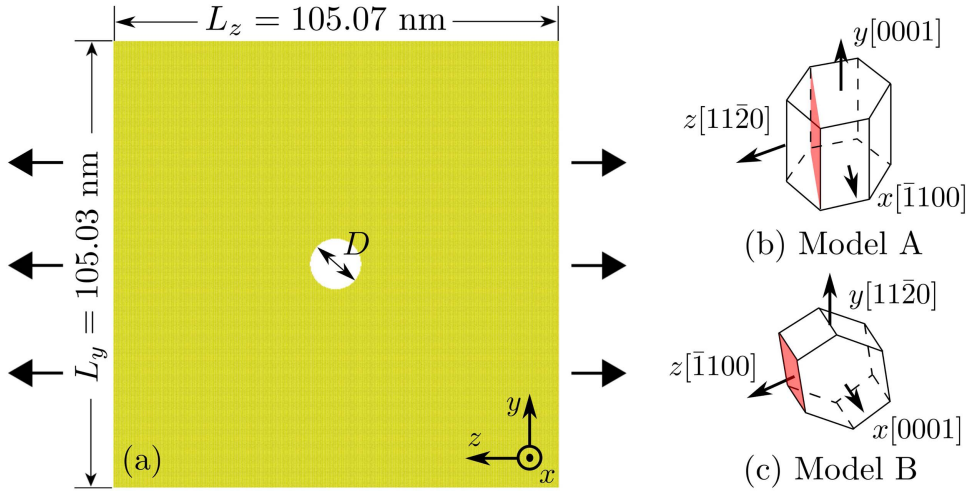

Figure 1. (a) Simulation cell of a Mg single crystal containing a cylindrical void. Thickness of the model in one supercell $L_x = 14.34$ nm. The void diameter D varies from 2, 6, 12, 18, 24, to 30 nm. Two sets of crystallographic orientations—(b) $x[\bar{1}100]$–$y[0001]$–$z[11\bar{2}0]$ and (c) $x[0001]$–$y[11\bar{2}0]$–$z[\bar{1}100]$—are employed. In (b), (c), the planes perpendicular to the tensile loading direction, i.e., the z direction, are highlighted in red.

voids affect the mechanical behavior of materials differently [12, 23], physical understanding of voided materials cannot be obtained by extrapolating from that of cracked ones.

While the effects of model size [20], initial porosity [21, 22], strain rate [20–22], temperature [20, 22], crystallographic orientations [20], and interatomic potential [22] have been investigated in voided Mg single crystals, the question remains as to how the initial porosity affects the material deformation in cases of different crystallographic orientations; an exploration of this would shed light on the significance of the elastic anisotropy of materials, a factor often overlooked in previous continuum models. Thus, in this paper, we perform large scale MD simulations to analyze deformation of Mg single crystals containing periodic cylindrical nanovoids as a function of the initial porosity and crystallographic orientations. Since the validity of atomistic-based simulation results heavily hinges on the selection of the interatomic potential [24–26], two potentials are employed with their results compared side-by-side.

2. Methodology

The simulation cell of a Mg single crystal with an initially cylindrical void at the center is shown in figure 1(a). Periodic boundary conditions are applied along all three directions, in effect creating a Mg single crystal with periodic nanovoid structures. Each cuboidal model, containing about 7 million atoms, has edge sizes of $L_x = 14.34$ nm, $L_y = 105.03$ nm, and $L_z = 105.07$ nm. Two sets of crystallographic orientations are employed: $x[\bar{1}100]$–$y[0001]$–$z[11\bar{2}0]$ and $x[0001]$–$y[11\bar{2}0]$–$z[\bar{1}100]$, referred to as models A and B, respectively. In the two models, the tensile loading direction, i.e., the z direction, is perpendicular to two types of prismatic planes, which are highlighted in red in figures 1(b), (c). The two orientations are chosen because they correspond to the lowest (model A) and the highest (model B) resistances to fatigue crack growth in mode I fracture of Mg among all 10 orientations of interest in the HCP structure [16]. The void diameter D varies from 2 nm, 6 nm, 12 nm, 18 nm, 24 nm, to 30 nm, corresponding to the initial porosity $f_0 = 0.03\%, 0.26\%, 1.02\%, 2.31\%, 4.10\%$, and 6.4%, respectively.

Atomistic simulations are conducted using LAMMPS [27]. First, dynamic relaxation at 10 K with an NPT ensemble is performed for 20 ps for the specimen to reach an equilibrium state subject to zero external loading. Then the configuration is energy minimized by iteratively adjusting atoms' positions using the conjugate gradient algorithm. It follows that a homogeneous uniaxial tension is applied on the model along the z axis with an engineering strain rate $\dot{\varepsilon}_{zz} = 10^9\ \mathrm{s}^{-1}$ until the engineering strain $\varepsilon_{zz} = 0.15$ is reached; the engineering stress σ_{zz} is calculated using the virial theorem. A constant temperature of 10 K and zero transverse stresses along the x and y directions are maintained with an NPT ensemble. We remark that since the mechanical responses for the two selected crystallographic orientations weakly depend on the temperature [16] and the nanovoid growth mechanism does not change with the strain rate between 10^7 and $10^{10}\ \mathrm{s}^{-1}$ [20–22], our simulation results are representative of those at a wide range of temperatures and strain rates. In all dynamic simulations, the time step is 2 fs. Two interatomic potentials—the embedded atom method (EAM) potential by Sun *et al* [28] and the modified embedded atom method (MEAM) potential by Wu *et al* [29], which are considered the most accurate

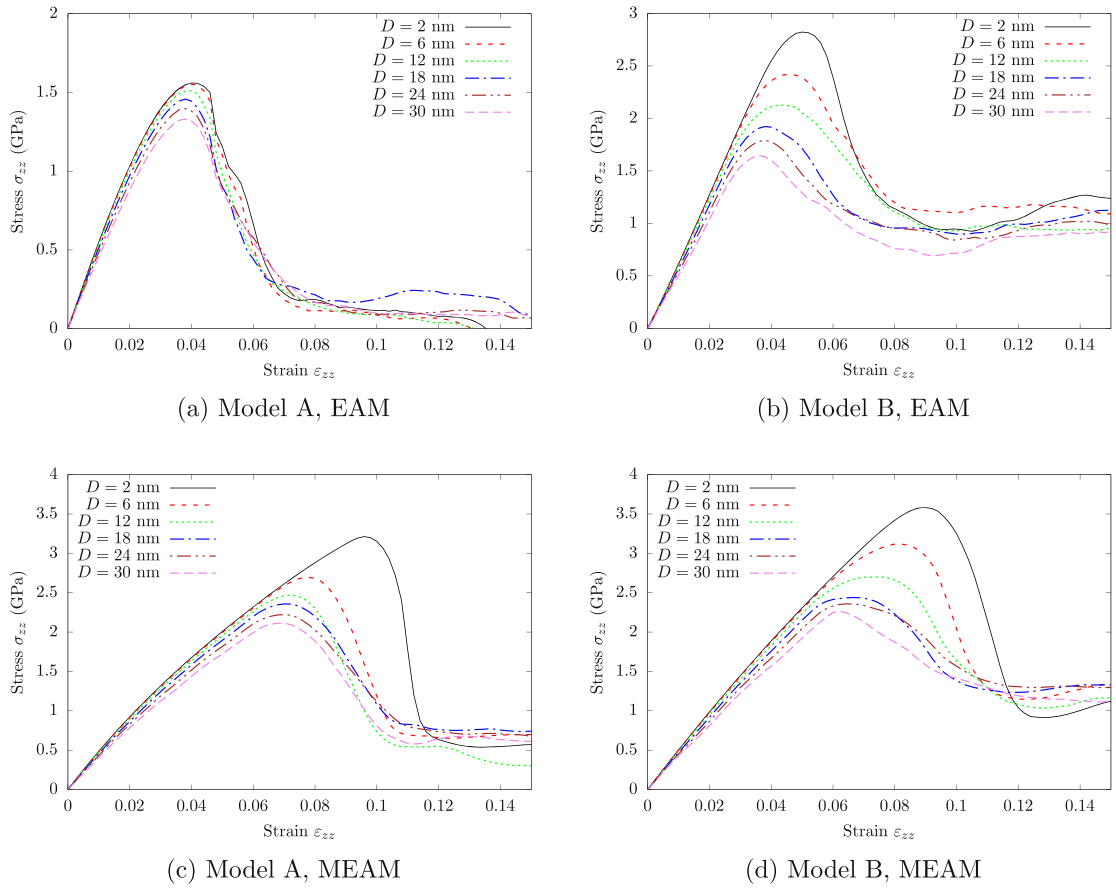

Figure 2. Initial void diameter D-dependent stress–strain curves for models A and B with EAM and MEAM potentials.

in terms of the dislocation core description among all EAM and MEAM potentials for Mg, respectively [29, 30] —are adopted for interactions between Mg atoms. The lattice constant a and the c/a ratio are 3.184 and 1.628 using the EAM potential, while 3.187 and 1.623 using the MEAM potential. Simulation results are visualized using OVITO [31], with the defects identified by the polyhedral template matching (PTM) method [32].

3. Stress–strain response

Stress–strain curves for models A and B with EAM and MEAM potentials, with varying initial void diameter D, are plotted in figure 2. When $D = 2$ nm, Young's modulus E at $\varepsilon_{zz} = 0.01$ of model A is 53.17 GPa (EAM) and 46.6 GPa (MEAM), while that of model B is 63.92 GPa (EAM) and 49.38 GPa (MEAM). Because a Mg single crystal has a low elastic anisotropy index [33], it is safe to assume that it is elastic transverse isotropic. In the meantime, since the two planes normal to the loading direction in two models are different types of prismatic planes, the average Young's modulus along the transverse direction (i.e., within the basal plane) is 58.545 GPa and 47.99 GPa for EAM and MEAM potentials, respectively. On the other hand, it is known that the Young's modulus along the same direction in an elastic transverse isotropic media is [34]

$$E = \frac{c_{11}^2 c_{33} + 2c_{13}^2 c_{12} - 2c_{11}c_{13}^2 - c_{33}c_{12}^2}{c_{11}c_{33} - c_{13}^2}, \tag{1}$$

where $c_{ij}(i, j = 1, 2, 3)$ are elastic constants, with $c_{11} = 69.6$ GPa (EAM) and 64.3 GPa (MEAM), $c_{12} = 25.3$ GPa (EAM) and 25.5 GPa (MEAM), $c_{13} = 16$ GPa (EAM) and 20.3 GPa (MEAM), and $c_{33} = 69.5$ GPa (EAM) and 70.9 GPa (MEAM). As a result, $E = 58.83$ GPa and 51.86 GPa for EAM and MEAM potentials, respectively, which are close to our MD simulation results.

The yield stresses σ_Y, taken at the initiation of lattice defects, are summarized in figure 3. Also shown are results from an analytic model proposed by Lubarda *et al* [35], i.e.,

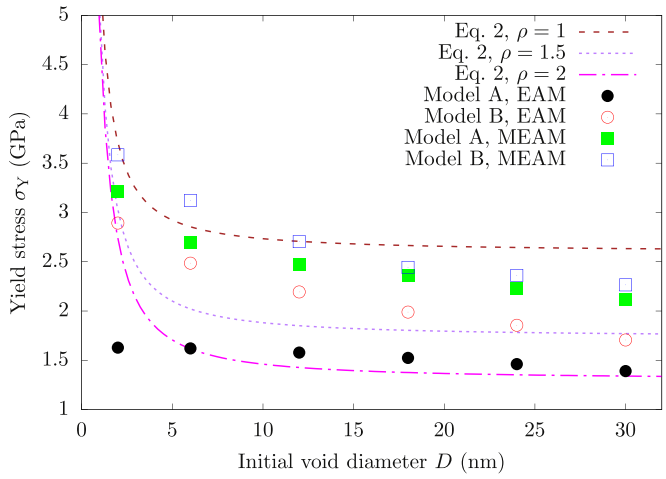

Figure 3. Yield stress σ_Y as a function of the initial void diameter D for models A and B with EAM and MEAM potentials. Analytic predictions based on the Lubarda model [35] in equation (2) are also shown with $\rho = 1$, $\rho = 1.5$, and $\rho = 2$.

$$\sigma_c = \frac{\sqrt{2}\,bG}{\pi D(1-\nu)} \frac{(1+2\sqrt{2}\,\rho b/D)^4 + 1}{(1+2\sqrt{2}\,\rho b/D)^4 - 1}, \tag{2}$$

where b is the magnitude of the Burgers vector of the dislocation, G is the isotropic shear modulus, ν is the Poisson's ratio, and ρ is an adjustable parameter with which $\rho\, b$ is the dislocation width. In our case, the two interatomic potentials give, on average, $b = 0.31855$ nm, $G = 25.4$ GPa, and $\nu = 0.22$, whereas b is for the $\langle a \rangle$ dislocation on the prismatic plane which, as will be discussed in the next section, is the only type of dislocations nucleated from the void surface. We remark that the Lubarda model is based on the assumption that only edge dislocations are nucleated from the void surface within an elastic isotropic 2D media subject to uniform biaxial tension under the plane strain condition.

In all cases, a larger D leads to a lower σ_Y, in agreement with the predictions of the Lubarda model [35] between $\rho = 1$ and $\rho = 2$. Both interatomic potentials predict that, with the same D, model B has a higher yield stress than model A, in line with a previous finding that the former has a higher fatigue crack resistance than the latter [16]. For the same model with the same D, the MEAM potential always results in a higher yield stress than the EAM potential. In other words, the MEAM-based predictions are closer to the Lubarda model with $\rho = 1$, while the EAM-based ones are closer to that with $\rho = 2$. On the other hand, previous studies [30, 36] found that the two interatomic potentials predict very similar core structures of dislocations on the prismatic plane, i.e., $\rho \approx 1.5$. Thus, the difference in their yield stress must be attributed to factors other than the dislocation width, suggesting that the Lubarda model with only one adjustable parameter is oversimplified.

4. Defect formation and void evolution

In model A, at the yield point, two types of tension twins—TT_1 and TT_2, characterized by the twin plane as illustrated in figures 4(c) and (g)—are observed. With the EAM potential, TT_2 on $(\bar{1}2\bar{1}1)$ and $(\bar{2}111)$ planes are nucleated from the void surface, except that when $D = 2$ nm, the tension twins are nucleated homogeneously inside the spcimen, as shown in figure 4(a). We remark this exception corresponds to the noticeble deviation of the yield stress for $D = 2$ nm from the Lubarda model prediction compared with the cases of other D (figure 3). For all D, the formation of TT_2 is accompanied by the HCP $\rightarrow$ BCC phase transformation. With the MEAM potential, however, $\langle a \rangle$ edge dislocations on two prismatic planes $(\bar{1}010)$ and $(01\bar{1}0)$ are nucleated from the top and bottom sites of the void surface, before some HCP atoms are transformed to an FCC structure. It follows that Shockley partial dislocations are nucleated inside the FCC region, resulting in TT_1 on $(01\bar{1}2)$ and $(\bar{1}012)$ planes. The coexistence of HCP $\rightarrow$ FCC phase transformation and TT_1 was also reported in two other HCP metals: Zr [37] and Ti [38].

The occurrence of phase transformation and twinning violates the assumption of the Lubarda model that the yielding is solely controlled by the nucleation of edge dislocations from the void surface, yet the analytic predictions inexplicably do not fall too far from the simulation results. Reference [29] studied the TT_1 dislocation using the MEAM potential and found the result in remarkable agreement with the density functional theory calculation. However, we are not aware of any previous investigation of the tension twin using the EAM

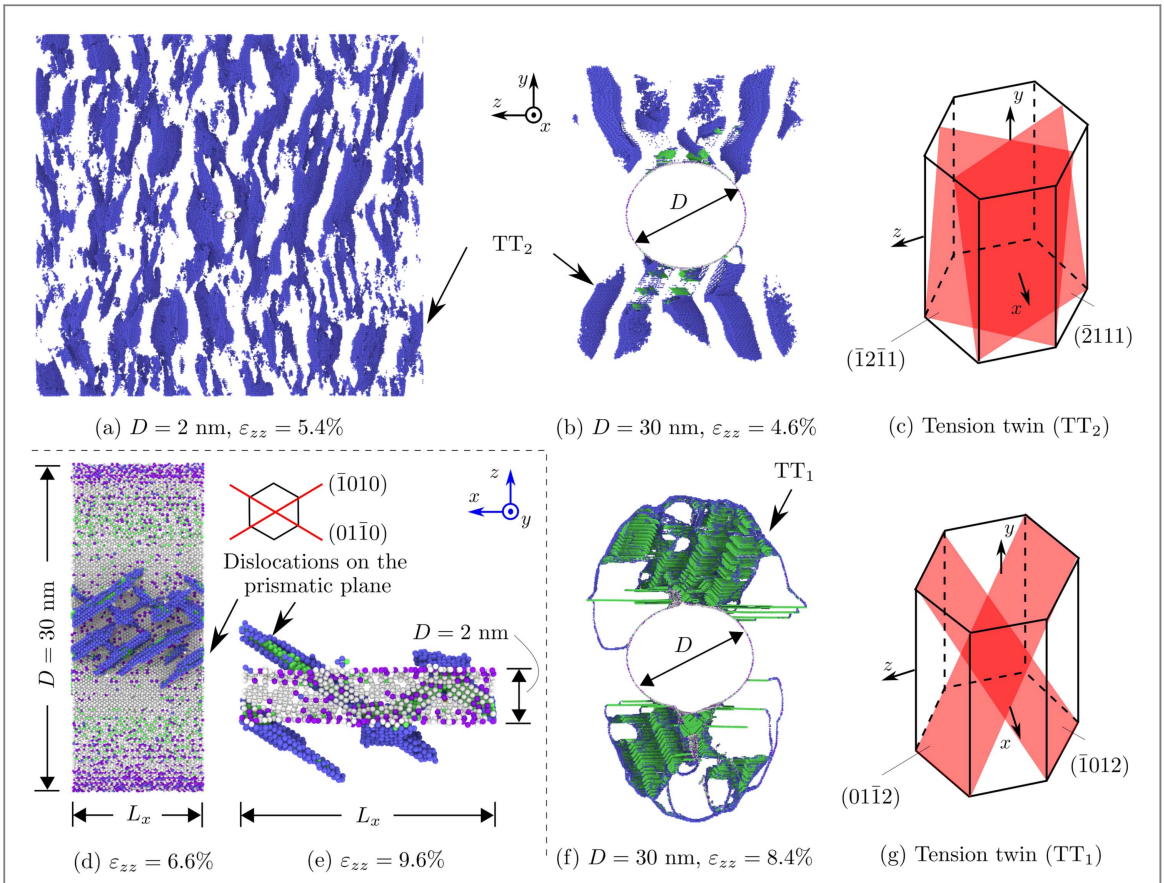

Figure 4. Snapshots of atomic configurations in model A with (a), (b) EAM and (d)–(f) MEAM interatomic potentials. The views for (a), (b), (f) and (d), (e) are illustrated by the black and blue coordinate systems, respectively. Atoms are colored using the PTM method [32], with FCC, BCC, simple cubic, and unknown local structures in green, blue, magenta, and white, respectively; all HCP atoms are deleted. Two types of tension twins—TT_1 and TT_2—are illustrated in (g) and (c), respectively.

potential by Sun *et al* [28]. As a result, we are not able to explain the difference in the tension twin formation between the two interatomic potentials. On the other hand, we note that prior MD simulations [39] using another EAM potential [40] reported that homogeneous nucleation of TT_1 in a Mg single crystal requires a higher critical resolved shear stress (1.5 GPa) than that of TT_2 (0.8 GPa), in alignment with our finding that the MEAM potential predicts a higher yield stress than the EAM potential.

In model B, at the yield point, both EAM and MEAM potentials predict that $\langle a \rangle$ edge dislocations on two prismatic planes $(\bar{1}010)$ and $(01\bar{1}0)$ are nucleated from the top and bottom sites of the void surface, as shown in figure 5. No twins are observed at higher strains. Between the two potentials, at 0 K, the Peierls stresses of the edge dislocation on the prismatic plane are 13 and 9.3 MPa using the EAM [30] and MEAM potentials [29], respectively, in contrast to our simulation results that the former leads to a lower yield stress than the latter. This indicates that other quantities, such as the critical stress required to nucleate the dislocation from the void surface, need to be taken into account to justify the potential-dependent difference.

To better examine the void growth, we calculate the porosity, which is found to increase sharply once the defects, either dislocations or twinning, are nucleated, except in model A with $D = 2$ nm using the EAM potential. As described earlier, in this exceptional case (figure 4(a)), tension twins are nucleated homogeneously within the specimen, instead of from the void surface. Subject to further straining, these twins push the materials around the void inward, and reduce the void size/porosity, as illustrated by the black solid line in figure 6. For other D in model A, the void continues growing and maintains a near-elliptic shape up to the maximum strain of 0.15. In model B, as more dislocations glide outward, extrusions are formed and grow at the top and bottom sites of the void. For $D = 2$ nm, the extrusions are large enough to close the central part of the void, resulting in two voids, as shown in figure 5(f), as well as a decrease in the void size, as illustrated by the blue dash–dot line and blue open squares in figure 6. For larger D, there is still one void, yet the extrusions significantly reduce the length of the minor axes (along the y direction) of the elliptic void and the void size growth rate.

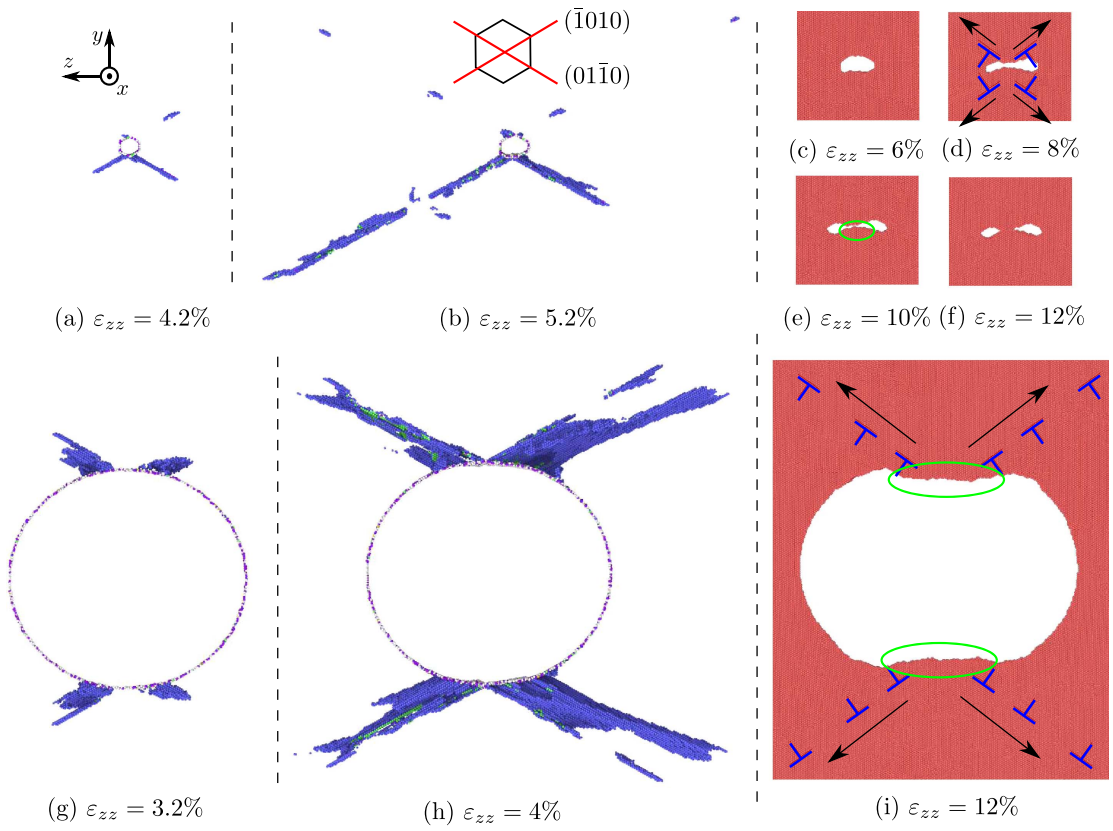

Figure 5. Snapshots of atomic configurations in model B with the EAM potential for (a)–(f) $D = 2$ nm and (g)–(i) $D = 30$ nm. The view is illustrated by the coordinate system in (a). In (a), (b), (g), and (h), atoms are colored in the same way as in figure 4, with all HCP atoms deleted. The extrusions at the void surface are marked by green circles in (e) and (i).

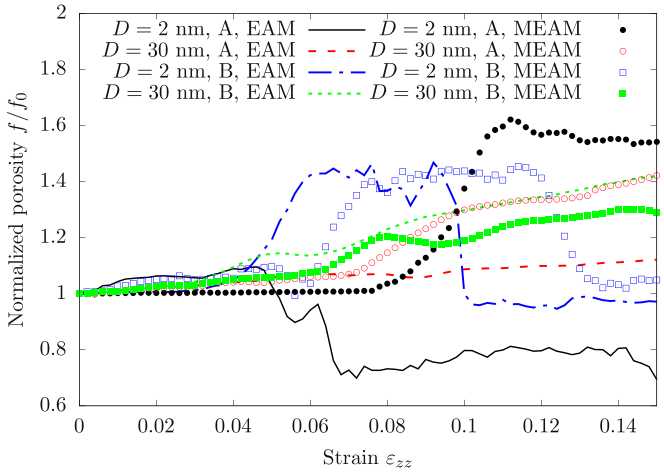

Figure 6. Evolution of porosity f normalized by the initial porosity f_0, for void diameter $D = 2$ nm and 30 nm in models A and B with EAM and MEAM interatomic potentials.

5. Conclusion

In this paper, we perform large scale MD simulations to explore initial porosity-, crystallographic orientation-, and interatomic potential-dependent deformation of periodic nanovoid structures in Mg single crystals subject to uniaxial tension along the z direction. Investigations are conducted in the context of stress–strain response, defect formation, and void evolution. The calculated yield stresses are compared with a local continuum-based analytic prediction, whose applicability is also discussed. Main results are summarized as follows:

(i) For the two models with different crystallographic orientations, both EAM and MEAM potentials predict a lower yield stress for a larger initial void, in reasonably good agreement with the analytic model. For the same initial porosity and orientations, the MEAM potential results in a higher yield stress than the EAM potential.

(ii) In model A, with $x[\bar{1}100]$–$y[0001]$–$z[11\bar{2}0]$ orientations, the first and second types of tension twins, accompanied by HCP → FCC and HCP → BCC phase transformation, are nucleated from the void surface using the MEAM and EAM potentials, respectively. The exception is that when $D = 2$ nm, the EAM potential predicts homogeneous nucleation of tension twins within the specimen, instead of from the void surface; as a result, the void size decreases after yielding in this particular case. For other D, the void size increases sharply on the threshold of plasticity and continues growing up to the maximum strain while the void maintains a near elliptic shape.

(iii) In model B, with $x[0001]$–$y[11\bar{2}0]$–$z[\bar{1}100]$ orientations, both EAM and MEAM potentials predict that $\langle a \rangle$ edge dislocations on the prismatic planes are nucleated from the void surface. As more dislocations glide away from the void, extrusions are formed at its top and bottom sites. When $D = 2$ nm, the extrusions are large enough to pinch the void into two voids. For other D, the void size remains approximately invariant after certain strain, with its minor axis along the transverse y direction much shorter than that in model A.

Besides bringing new physical understanding of materials with periodic nanovoid structures, our work emphasizes the significance of the interatomic potential in atomistic modeling, which is a powerful tool but also a dangerous one, as it is very easy to set up a simulation 'incorrectly'. In practice, researchers usually seek to employ the best potential to minimize the 'incorrectness'. However, it is not always clear which potential is the best because they were, more often than not, fit to limited experimental and *ab initio* data while the quantities relevant for desired simulations may not be considered. Thus, the 'incorrectness' may be regarded as variability arising from uncertainty in model parameters. Indeed, the issue of uncertainty quantification and propagation is vitally important even for skilled atomistic modelers, and one of the key points of this paper is to shed light on implications for variability of predictions related to nanovoid structures.

Acknowledgments

We thank Dr. Zhaoxuan Wu for providing the MEAM potential file for Mg. The work of SX was supported in part by the Elings Prize Fellowship in Science offered by the California NanoSystems Institute (CNSI) on the UC Santa Barbara campus. SX also acknowledges support from the Center for Scientific Computing from the CNSI, MRL: an NSF MRSEC (DMR-1121053). SZC would like to express his sincere gratitude for the financial support from the AVIC Center for Materials Characterisation, Processing and Modelling at Imperial College London. This work used the Extreme Science and Engineering Discovery Environment (XSEDE), which is supported by National Science Foundation grant number ACI-1053575.

ORCID iDs

Shuozhi Xu https://orcid.org/0000-0003-0121-9445

References

[1] Xu S Z, Hao Z M and Wan Q 2010 A molecular dynamics study of void interaction in copper *IOP Conf. Ser.: Mater. Sci. Eng.* **10** 012175
[2] Xu S Z, Hao Z M, Su Y Q, Hu W J, Yu Y and Wan Q 2012 Atomic collision cascades on void evolution in vanadium *Radiat. Eff. Defects Solids* **167** 12–25
[3] Xiong L, Xu S, McDowell D L and Chen Y 2015 Concurrent atomistic-continuum simulations of dislocation-void interactions in fcc crystals *Int. J. Plast.* **65** 33–42
[4] Ashby M F 1970 The deformation of plastically non-homogeneous materials *Phil. Mag.* A **21** 399–424
[5] Gurson A L 1977 Continuum theory of ductile rupture by void nucleation and growth: I. Yield criteria and flow rules for porous ductile media *J. Eng. Mater. Technol.* **99** 2–15
[6] Cui Y and Chen Z 2016 Material transport via the emission of shear loops during void growth: a molecular dynamics study *J. Appl. Phys.* **119** 225102
[7] Cui Y and Chen Z T 2017 Void growth via atomistic simulation: will the formation of shear loops still grow a void under different thermo-mechanical constraints? *Phil. Mag.* **97** 3142–71
[8] Nguyen L D and Warner D H 2012 Improbability of void growth in aluminum via dislocation nucleation under typical laboratory conditions *Phys. Rev. Lett.* **108** 035501
[9] Xu S Z, Hao Z M, Su Y Q, Yu Y, Wan Q and Hu W J 2011 An analysis on nanovoid growth in body-centered cubic single crystalline vanadium *Comput. Mater. Sci.* **50** 2411–21

[10] Su Y and S Xu 2016 On the role of initial void geometry in plastic deformation of metallic thin films: a molecular dynamics study *Mater. Sci. Eng.*: A **678** 153–64
[11] Xu S and Su Y 2016 Nanovoid growth in bcc α-Fe: influences of initial void geometry *Modelling Simul. Mater. Sci. Eng.* **24** 085015
[12] Xu S, Su Y, Chen D and Li L 2017 Plastic deformation of Cu single crystals containing an elliptic cylindrical void *Mater. Lett.* **193** 283–7
[13] Bringa E M, Traiviratana S and Meyers M A 2010 Void initiation in fcc metals: effect of loading orientation and nanocrystalline effects *Acta Mater.* **58** 4458–77
[14] Bhatia M A, Solanki K N, Moitra A and Tschopp M A 2013 Investigating damage evolution at the nanoscale: molecular dynamics simulations of nanovoid growth in single-crystal aluminum *Metall. Mater. Trans.* A **44** 617–26
[15] Wang J P, Yue Z F, Wen Z X, Zhang D X and Liu C Y 24, 2017 Orientation effects on the tensile properties of single crystal nickel with nanovoid: atomistic simulation *Comput. Mater. Sci.* **132** (Suppl. C) 116–24
[16] Tang T, Kim S and Horstemeyer M F 2010 Fatigue crack growth in magnesium single crystals under cyclic loading: molecular dynamics simulation *Comput. Mater. Sci.* **48** 426–39
[17] Wu Z and Curtin W A 2015 Brittle and ductile crack-tip behavior in magnesium *Acta Mater.* **88** (Suppl. C) 1–12
[18] Rawat S and Joshi S P 2016 Effect of multiaxial loading on evolution of $\{10\bar{1}2\}$ twinning in magnesium single crystals *Mater. Sci. Eng.* A **659** (Suppl. C) 256–69
[19] Yashiro K 2017 Local lattice instability analysis on mode I crack tip in hcp-Mg: unstable mode for crack propagation versus dislocation emission *Comput. Mater. Sci.* **131** (Suppl. C) 220–9
[20] Tang T, Kim S and Horstemeyer M F 2010 Molecular dynamics simulations of void growth and coalescence in single crystal magnesium *Acta Mater.* **58** 4742–59
[21] Ponga M, Ramabathiran A A, Bhattacharya K and Ortiz M 2016 Dynamic behavior of nano-voids in magnesium under hydrostatic tensile stress *Modelling Simul. Mater. Sci. Eng.* **24** 065003
[22] Grégoire C and Ponga M 2017 Nanovoid failure in magnesium under dynamic loads *Acta Mater.* **134** (Suppl. C) 360–74
[23] Aghababaei R and Joshi S P 2014 Micromechanics of tensile twinning in magnesium gleaned from molecular dynamics simulations *Acta Mater.* **69** (Suppl. C) 326–42
[24] Xu S, Xiong L, Chen Y and McDowell D L 2017 Comparing EAM potentials to model slip transfer of sequential mixed character dislocations across two symmetric tilt grain boundaries in Ni *JOM* **69** 814–21
[25] Xu S, Startt J K, Payne T G, Deo C S and McDowell D L 2017 Size-dependent plastic deformation of twinned nanopillars in body-centered cubic tungsten *J. Appl. Phys.* **121** 175101
[26] Chavoshi S Z, Xu S and Goel S 2017 Addressing the discrepancy of finding the equilibrium melting point of silicon using molecular dynamics simulations *Proc. R. Soc.* A **473** 20170084
[27] Plimpton S 1995 Fast parallel algorithms for short-range molecular dynamics *J. Comput. Phys.* **117** 1–19
[28] Sun D Y, Mendelev M I, Becker C A, Kudin K, Haxhimali T, Asta M, Hoyt J J, Karma A and Srolovitz D J 2006 Crystal-melt interfacial free energies in hcp metals: a molecular dynamics study of Mg *Phys. Rev.* B **73** 024116
[29] Wu Z, Francis M F and Curtin W A 2015 Magnesium interatomic potential for simulating plasticity and fracture phenomena *Modelling Simul. Mater. Sci. Eng.* **23** 015004
[30] Yasi J A, Nogaret T, Trinkle D R, Qi Y, Hector L G Jr and Curtin W A 2009 Basal and prism dislocation cores in magnesium: comparison of first-principles and embedded-atom-potential methods predictions *Modelling Simul. Mater. Sci. Eng.* **17** 055012
[31] Stukowski A 2010 Visualization and analysis of atomistic simulation data with OVITO—the open visualization tool *Modelling Simul. Mater. Sci. Eng.* **18** 015012
[32] Larsen P M, Schmidt S and Schiøtz J 2016 Robust structural identification via polyhedral template matching *Modelling Simul. Mater. Sci. Eng.* **24** 055007
[33] Ranganathan S I and Ostoja-Starzewski M 2008 universal elastic anisotropy index *Phys. Rev. Lett.* **101** 055504
[34] Bower A F 2009 *Applied Mechanics of Solids* 1 edn (Boca Raton, FL: CRC Press)
[35] Lubarda V A, Schneider M S, Kalantar D H, Remington B A and Meyers M A 2004 Void growth by dislocation emission *Acta Mater.* **52** 1397–408
[36] Shin I and Carter E A 2012 Orbital-free density functional theory simulations of dislocations in magnesium *Modelling Simul. Mater. Sci. Eng.* **20** 015006
[37] Kucherov L and Tadmor E B 2007 Twin nucleation mechanisms at a crack tip in an hcp material: molecular simulation *Acta Mater.* **55** 2065–74
[38] Ren J, Sun Q, Xiao L, Ding X and Sun J 2014 Phase transformation behavior in titanium single-crystal nanopillars under [0001] orientation tension: a molecular dynamics simulation *Comput. Mater. Sci.* **92** (Suppl. C) 8–12
[39] Fan H and El-Awady J A 2015 Molecular dynamics simulations of orientation effects during tension, compression, and bending deformations of magnesium nanocrystals *J. Appl. Mech.* **82** 101006
[40] Liu X-Y, Adams J B, Ercolessi F and Moriarty J A 1996 EAM potential for magnesium from quantum mechanical forces *Modelling Simul. Mater. Sci. Eng.* **4** 293